Solid-State Electronics Vol. 35, No. 9, pp. 1291–1298, 1992
Printed in Great Britain

0038-1101/92 $5.00 + 0.00
Pergamon Press Ltd

LONG-CHANNEL SILICON-ON-INSULATOR MOSFET THEORY

A. ORTIZ-CONDE,[1] R. HERRERA,[1] P. E. SCHMIDT,[2] F. J. GARCÍA SÁNCHEZ[1] and J. ANDRIAN[2]

[1]Departamento de Electrónica, Universidad Simón Bolívar, Apartado 89000, Caracas 1080-A, Venezuela
[2]Department of Electrical and Computer Engineering, Florida International University, University Park, Miami, FL 33199, U.S.A.

(Received 30 September 1991; in revised form 13 January 1992)

Abstract—Based on the procedure of Pierret and Shields [1, *Solid-St. Electron.* **26**, 143, 1983] for the long-channel bulk MOSFET, a new single-integral expression is obtained to describe the current–voltage characteristics for the silicon-on-insulator (SOI) MOSFET. This expression is valid for: any degree of inversion, all back-gate bias conditions and any semiconductor film thickness. Our single-integral expression, applied to a given back-gate bias condition and using the appropriate approximations, can be simplified to the results of the previous models.

NOTATION

I_D	drain current (A)
I_{Dsat}	drain saturation current (A)
V_D	voltage between the drain and the source (V)
V_{GSf}	voltage between the front-gate and the source (V)
V_{GSb}	voltage between the back-gate and the source (V)
V_{FB}^f	front-gate (conventional) flatband voltage (V)
V_{FB}^b	back-gate (conventional) flatband voltage (V)
V_{Gf}	front-gate voltage with the flatband voltage included ($V_{Gf} \equiv V_{GSf} - V_{FBf}$)
V_{Gb}	back-gate voltage with the flatband voltage included ($V_{Gb} \equiv V_{GSb} - V_{FBb}$)
V	electron quasi-Fermi potential along the channel (V)
V_{Tf}	front-gate threshold voltage (V)
U	electrostatic potential (V)
U_{sf}	front-surface potential (V)
U_{sb}	back-surface potential (V)
U_{sf0}	front-surface potential at the source (V)
U_{sb0}	back-surface potential at the source (V)
U_{sfL}	front-surface potential at the drain (V)
U_{sbL}	back-surface potential at the drain (V)
ϕ_B	Fermi potential [$\phi_B = (kT/q)\ln(N_A/n_i)$]
F	electric field normal to the surface ($V \cdot cm^{-1}$)
F_{sf}	front-surface electric field ($V \cdot cm^{-1}$)
F_{sb}	back-surface electric field ($V \cdot cm^{-1}$)
F_{sf0}	front-surface electric field at the source ($V \cdot cm^{-1}$)
F_{sb0}	back-surface electric field at the source ($V \cdot cm^{-1}$)
F_{sfL}	front-surface electric field at the drain ($V \cdot cm^{-1}$)
F_{sbL}	back-surface electric field at the drain ($V \cdot cm^{-1}$)
F_{sfda}	depletion front-surface electric field ($V \cdot cm^{-1}$)
α	variable that relates the interaction between the front- and the back-gates ($V^2 \cdot cm^{-2}$)
α_0	value of variable α at the source, for which $y = 0$ and $V = 0$ ($V^2 \cdot cm^{-2}$)
α_L	value of variable α at the drain, for which $y = L$ and $V = V_D$ ($V^2 \cdot cm^{-2}$)
μ_n	effective electron mobility ($cm^2 \cdot V^{-1} \cdot s^{-1}$)
N_A	film doping density (cm^{-3})
n	electron concentration (cm^{-3})
p	hole concentration (cm^{-3})
n_0	thermal equilibrium electron carrier density (cm^{-3})
p_0	thermal equilibrium hole carrier density (cm^{-3})
n_i	intrinsic carrier concentration (cm^{-3})
Q_n	total channel charge density per unit area ($C \cdot cm^{-2}$)
Q_b	body depletion charge ($Q_b = -qN_A t_b$)
C_{of}	front-gate oxide capacitance per unit area ($F \cdot cm^{-2}$)
C_{ob}	back-gate oxide capacitance per unit area ($F \cdot cm^{-2}$)
C_b	depletion capacitance per unit area ($F \cdot cm^{-2}$)
C_{bb}	effective body capacitance which is the series combination of C_{ob} and C_b [$C_{bb} = C_{ob}C_b/(C_{ob} + C_b)$]
x	coordinate perpendicular to the channel (cm)
y	coordinate along the channel (cm)
Z	channel width (cm)
L	channel length (cm)
t_b	semiconductor film thickness (cm)
L_D	extrinsic Debye length (cm)
ϵ_s	semiconductor permittivity ($F \cdot cm^{-1}$)
k	Boltzmann's constant ($C \cdot V \cdot K^{-1}$)
T	absolute temperature (K)
q	magnitude of electron charge (C)
β	inverse of the thermal voltage ($\beta \equiv q/kT$)

1. INTRODUCTION

The fundamental advantages of silicon-on-insulator (SOI) structures over conventional bulk MOSFET devices have motivated many recent publications[2–14]. Some of these advantages are: suppression of latch-up, 3-D integration, reduction of short-channel effects and mobility enhancement. Thin-film SOI MOSFETs present charge coupling effects between front- and back-gates. As a result, the analytical formulation of the current–voltage characteristic for these devices is more difficult to model than for conventional bulk MOSFET devices.

In 1978, the charge sheet model[15–18] for the long-channel bulk MOSFET was successful in predicting the current–voltage characteristics within 5% of those obtained by the Pao–Sah exact model[19]. The importance of the charge sheet model derives from its validity for all bias conditions and its simplicity for numerical calculations because it does not contain any integral expression. In 1983, Pierret and Shields[1] transformed the double-integral expression of Pao–Sah's model, without carrying out any approximation, into a completely equivalent

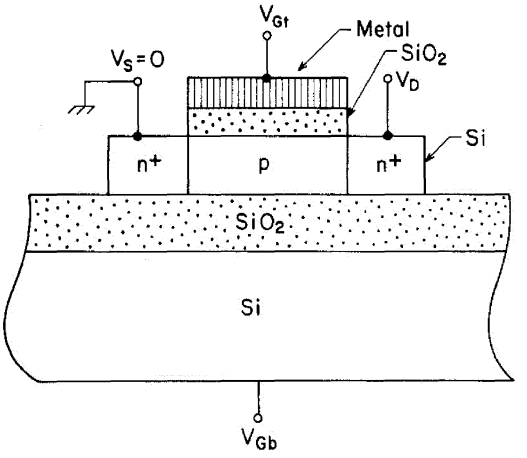

Fig. 1. Cross-section of the four-terminal n-channel inversion mode SOI MOSFET.

single-integral relationship. This general single-integral relationship can be simplified to the charge sheet model by using the appropriate approximations.

Lim and Fossum[2,7] have developed an analytical model of the long-channel SOI MOSFET to describe the effects of charge coupling between the front- and back-gates in strong inversion. The charge sheet ideas[15–18] for the long-channel bulk MOSFET, which are valid for all inversion conditions and do not require many calculations, have inspired recent work[8–13] to generate analogous models for the long-channel thin-film MOSFET. The first of these articles, published in 1988[8], presented the foundation of a charge-sheet model for the SOI MOSFET. In 1989, this first model was extended[9] to account for the nonequilibrium condition, and it was verified[10] for the case in which the electric field inside the thin film does change sign. The second model, developed by McKitterick and Caviglia in 1989[13], was based on the not generally valid assumption that the potential is constant across the complete Si film. The third model, presented by Mallikarjun and Bhat in 1990[3], was based on using depletion approximation along the complete Si film.

In spite of contemporary short-channel SOI technologies, long-channel and pseudo-long-channel models are useful as the basis for developing improved models for short-channel devices.

We summarize in Section 2.1 the rigorous analysis to calculate the surface potentials at the source and drain of the SOI MOSFET, without solving Poisson's equation completely, based on a nonlinear system of equations[8–12]. The effects of the Si substrate, as discussed by Flandre and Van de Wiele[20], have not been taken into account in the present model.

In Section 2.2, we present a new analytical rigorous formulation, analogous to Pao–Sah's model[19] for the bulk device, to describe the current–voltage characteristics of the long-channel SOI MOSFET. This model is based only on the gradual channel[21] and the quasi-equilibrium[9] approximations. This rigorous formulation, which is valid for all bias conditions and includes drift and diffusion currents, requires the numerical evaluation of a double-integral expression.

In Section 2.3, following a procedure analogous to Pierret and Shields[1] for the bulk device, we transform the double-integral expression, obtained in the previous section, into a completely equivalent single-integral relationship. This single-integral relationship, which reduces the computational times, is as general as the model contained in Section 2.2. We verify the predictions of our single-integral relationship with numerical calculations obtained from the double-integral expression.

In Section 3, we show how our general single-integral relationship, described in Section 2.3, can be reduced to: (i) the Pierret and Shields equation[1] for the bulk device if the Si film is very thick; (ii) Mallikarjun and Bhat's model[3] by using the depletion approximation; and (iii) Lim and Fossum's model[2] combining the strong inversion condition with the depletion approximation.

2. GENERAL THEORY

2.1. Calculation of the surface potentials

The gradual channel approximation[21] allows us to simplify the 2-D problem of the nonequilibrium long-channel thin-film MOSFET shown in Fig. 1, to a 1-D problem. Based on the quasi-equilibrium approximation[21], this 1-D analysis[9] for the nonequilibrium MOSFET leads to the numerical solution of the following four equations:

$$V_{Gf} = U_{sf} + \frac{\epsilon_s F_{sf}}{C_{of}}, \tag{1}$$

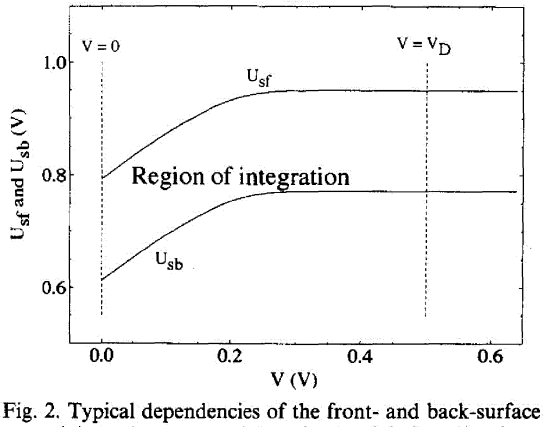

Fig. 2. Typical dependencies of the front- and back-surface potentials vs electron quasi-Fermi potential along the channel. The parameters used in this figure are: $V_{Gf} = 1.5$ V, $V_{Gb} = 0$, $C_{of} = 7.67 \times 10^{-8}$ F cm^{-2} (the front-gate oxide is 450 Å thick), $C_{ob} = 1.68 \times 10^{-9}$ F cm^{-2} (the back-gate oxide is 2.05 μm thick), $N_A = 3 \times 10^{16}$ cm^{-3} and $t_b = 880$ Å. We note that the region of integration in eqn (17) is between U_{sb} and U_{sf}, from $V = 0$ to $V = V_D$.

$$V_{Gb} = U_{sb} - \frac{\epsilon_s F_{sb}}{C_{ob}}, \tag{2}$$

$$F_{sf}^2 - G^2(U_{sf}, V) = F_{sb}^2 - G^2(U_{sb}, V) = \alpha \tag{3}$$

and

$$t_b = \int_{U_{sb}}^{U_{sf}} \frac{+dU}{F}, \tag{4}$$

with

$$V_{Gf} \equiv V_{GS}^f - V_{FB}^f,$$

and

$$V_{Gb} \equiv V_{GS}^b - V_{FB}^b,$$

and where V is the electron quasi-Fermi potential along the channel, U is the electrostatic potential, U_{sf} and U_{sb} are the front- and back-surface potentials, F_{sf} and F_{sb} are the front- and back-surface electric fields, C_{of} and C_{ob} are the front- and back-gate oxide capacitances, t_b is the semiconductor film thickness and α is a variable[8–12] that relates to the interaction between the front and back gates:

$$F = [\alpha + G^2(U, V)]^{1/2}, \tag{5}$$

is the electric field, and $G^2(U, V)$ is defined by:

$$G^2(U, V) = \frac{2}{\beta^2 L_D^2}\left[\exp(-\beta U) + \beta U - 1 + \frac{n_0}{p_0}\right.$$

$$\left.\{\exp(-\beta V)[\exp(\beta U) - 1] - \beta U\}\right]. \tag{6}$$

In eqn (6), p_0 and n_0 are the hole and electron thermal equilibrium carrier densities, $\beta = q/kT$ is the inverse of the thermal voltage, and

$$L_D = \left[\frac{\epsilon_s}{q\beta p_0}\right]^{1/2}, \tag{7}$$

is the extrinsic Debye length and the other symbols have their usual meaning.

The solution of the system of equations at the source, $V = 0$ for $y = 0$, gives: $U_{sf} = U_{sf0}$, $U_{sb} = U_{sb0}$, $F_{sf} = F_{sf0}$, $F_{sb} = F_{sb0}$ and $\alpha = \alpha_0$. Analogously, the solution at the drain, $V = V_D$ for $y = L$ where L is the channel length, yields: $U_{sf} = U_{sfL}$, $U_{sb} = U_{sbL}$, $F_{sf} = F_{sfL}$, $F_{sb} = F_{sbL}$ and $\alpha = \alpha_L$.

2.2. Pao–Sah's type model for the SOI MOSFET

The drain current, including drift and diffusion carrier transport in the Si, can be expressed by[21]:

$$I_D = -\mu_n \frac{Z}{L}\int_0^{V_D} Q_n \, dV, \tag{8}$$

where μ_n is the effective electron mobility, Z is the channel width and Q_n is the total inversion charge density inside the Si film. In contrast to the previous work[2,3], we do not separate Q_n into two contributions due to the front and back interfaces, $Q_n = Q_{nf} + Q_{nb}$, where Q_{nf} and Q_{nb} are the front and back inversion charge densities, respectively. The charge Q_n is calculated by[8–12]:

$$Q_n = -\int_{U_{sb}}^{U_{sf}} \frac{q(n - n_0)\, dU}{F}, \tag{9}$$

where

$$n = n_0 \exp(+\beta U - \beta V) \tag{10}$$

is the electron concentration.

An equivalent to Pao–Sah's equation for the SOI MOSFET is obtained by substituting eqn (9) into eqn (8):

$$I_D = +\mu_n \frac{Z}{L}\int_0^{V_D}\int_{U_{sb}}^{U_{sf}} \frac{q(n - n_0)\, dU}{F} dV. \tag{11}$$

2.3. Pierret and Shields's type model for the SOI MOSFET

Following the procedure developed by Pierret and Shields[1], we evaluate the partial derivative of eqn (5) and combine it with eqns (6), (7) and (10) to obtain:

$$\frac{\delta F}{\delta V} = \frac{1}{2F}\frac{d\alpha}{dV} - \frac{q(n - n_0)}{F\epsilon_s} - \frac{qn_0[1 - \exp(-\beta V)]}{F\epsilon_s}. \tag{12}$$

In above equation we have written $d\alpha/dV$ and not $\delta\alpha/\delta V$ because α does not depend on U. The substitution of eqn (12) into eqn (11) yields:

$$I_D = \mu_n \epsilon_s \frac{Z}{L}\int_0^{V_D}\int_{U_{sb}}^{U_{sf}}$$

$$\times\left\{\frac{1}{2F}\frac{d\alpha}{dV} - \frac{qn_0[1 - \exp(-\beta V)]}{F\epsilon_s} - \frac{\delta F}{\delta V}\right\} dU\, dV. \tag{13}$$

Let us define the integrals of the first, second and third terms of the above equation as I_1, I_2 and I_3, respectively, such that $I_D = I_1 + I_2 + I_3$. The first integral can be simplified to:

$$I_1 = +\mu_n \epsilon_s \frac{Z}{2L}\int_0^{V_D} \frac{d\alpha}{dV}\left[\int_{U_{sb}}^{U_{sf}} \frac{1}{F} dU\right] dV. \tag{14}$$

The term in the bracket in eqn (14) is just t_b because of eqn (4). Therefore, performing the integration in eqn (14), we obtain:

$$I_1 = +\mu_n \epsilon_s t_b \frac{Z}{2L}[\alpha_L - \alpha_0]. \tag{15}$$

The second term of the integration in eqn (13) gives:

$$I_2 = -\frac{\mu_n t_b q n_0 Z}{\beta L}[\beta V_D + \exp(-\beta V_D) - 1]. \tag{16}$$

Now we will calculate the term I_3, defined by:

$$I_3 = -\mu_n \epsilon_s \frac{Z}{L}\int_0^{V_D}\int_{U_{sb}}^{U_{sf}} \frac{\delta F}{\delta V} dU\, dV. \tag{17}$$

Following the ideas of Pierret and Shields[1] for the bulk device, we illustrate in Fig. 2 the dependence of U_{sf} and U_{sb} on V, for $V_{Gf} = 1.5$ V, $V_{Gb} = 0$, $C_{of} = 7.67 \times 10^{-8}$ F cm^{-2} (the front-gate oxide is 450 Å thick), $C_{ob} = 1.68 \times 10^{-9}$F cm^{-2} (the back-gate oxide is 2.05 μm thick), $N_A = 3 \times 10^{16}$ cm^{-3} and $t_b = 880$ Å. In this figure we see that the region of

integration is between U_{sb} and U_{sf}, from $V=0$ to $V=V_D$. This integration can be separated into four integrations:

$$\int_0^{V_D}\int_{U_{sb}}^{U_{sf}}\frac{\delta F}{\delta V}\,dU\,dV=\int_0^{V_D}\int_0^{U_{sf0}}\frac{\delta F}{\delta V}\,dU\,dV+\int_0^{V_D}\int_{U_{sf0}}^{U_{sf}}\frac{\delta F}{\delta V}\,dU\,dV-\int_0^{V_D}\int_0^{U_{sb0}}\frac{\delta F}{\delta V}\,dU\,dV-\int_0^{V_D}\int_{U_{sb0}}^{U_{sb}}\frac{\delta F}{\delta V}\,dU\,dV. \quad (18)$$

Since the first and the third terms in the above equation have constant limits of integration, the order of integration can be changed, yielding:

$$\int_0^{V_D}\int_0^{U_{sf0}}\frac{\delta F}{\delta V}\,dU\,dV=\int_0^{U_{sf0}}[F(U,V=V_D)-F(U,V=0)]dU \quad (19)$$

and

$$\int_0^{V_D}\int_0^{U_{sb0}}\frac{\delta F}{\delta V}\,dU\,dV=\int_0^{U_{sb0}}[F(U,V=V_D)-F(U,V=0)]\,dU \quad (20)$$

Now we change the order of the integration in the second term in eqn (18), by using Fig. 2 to identify the region involved:

$$\int_0^{V_D}\int_{U_{sf0}}^{U_{sf}}\frac{\delta F}{\delta V}\,dU\,dV=\int_{U_{sf0}}^{U_{sfL}}\int_{V_f}^{V_D}\frac{\delta F}{\delta V}\,dV\,dU, \quad (21)$$

where V_f is the value of V at which the front surface band-bending is U_{sf}. Then, we performed the integration in eqn (21) to obtain:

$$\int_0^{V_D}\int_{U_{sf0}}^{U_{sf}}\frac{\delta F}{\delta V}\,dU\,dV=\int_{U_{sf0}}^{U_{sfL}}[F(U,V=V_D)-F(U,V=V_f)]\,dU. \quad (22)$$

The fourth term in eqn (18), which is analogous to the second term, can be written as:

$$\int_0^{V_D}\int_{U_{sb0}}^{U_{sb}}\frac{\delta F}{\delta V}\,dU\,dV=\int_{U_{sb0}}^{U_{sbL}}[F(U,V=V_D)-F(U,V=V_b)]\,dU, \quad (23)$$

where V_b is the value of V at which the back-surface band-bending is U_{sb}.

The substitution of eqns (19), (20), (22) and (23) into eqn (18) gives:

$$\int_0^{V_D}\int_{U_{sb}}^{U_{sf}}\frac{\delta F}{\delta V}\,dU\,dV=\int_{U_{sbL}}^{U_{sfL}}F(U,V=V_D)\,dU-\int_{U_{sb0}}^{U_{sf0}}F(U,V=0)\,dU-\int_{U_{sf0}}^{U_{sfL}}F(U,V=V_f)\,dU+\int_{U_{sb0}}^{U_{sbL}}F(U,V=V_b)\,dU. \quad (24)$$

Since $U=U_{sf}$ for $V=V_f$, we recognize that $F(U,V=V_f)$ is just F_{sf}. Therefore, the third term of the previous equation is integrated using eqn (2):

$$\int_{U_{sf0}}^{U_{sfL}}F(U,V=V_f)\,dU=\frac{C_{of}}{\epsilon_s}[V_{Gf}(U_{sfL}-U_{sf0})-\tfrac{1}{2}(U_{sfL}^2-U_{sf0}^2)]. \quad (25)$$

Analogously, the fourth term of eqn (24) is:

$$\int_{U_{sb0}}^{U_{sbL}}F(U,V=V_b)\,dU=-\frac{C_{ob}}{\epsilon_s}[V_{Gb}(U_{sbL}-U_{sb0})-\tfrac{1}{2}(U_{sbL}^2-U_{sb0}^2)]. \quad (26)$$

Finally, the combination of eqns (13), (15–18) and (24–26) yields a general current–voltage equation valid for thin and thick SOI MOSFETs, and for all bias conditions:

$$I_D=+\mu_n\frac{Z}{L}\left\{C_{of}[V_{Gf}(U_{sfL}-U_{sf0})-\tfrac{1}{2}(U_{sfL}^2-U_{sf0}^2)]+Q_b\frac{n_i^2}{N_A^2}\frac{1}{\beta}[\beta V_D+\exp(-\beta V_D)-1]+\epsilon_s\int_{U_{sb0}}^{U_{sf0}}F(U,V=0)\,dU-\epsilon_s\int_{U_{sbL}}^{U_{sfL}}F(U,V=V_D)dU+\tfrac{1}{2}\epsilon_s t_b[\alpha_L-\alpha_0]+C_{ob}[V_{Gb}(U_{sbL}-U_{sb0})-\tfrac{1}{2}(U_{sbL}^2-U_{sb0}^2)]\right\}, \quad (27)$$

where Q_b is the body depletion charge ($Q_b=-qN_At_b$). For all practical doping concentrations the second term in eqn (27) is negligible.

We stress that the general single-integral expression in eqn (27) is completely equivalent to the double-integral expression presented in eqn (11). Therefore, eqn (27) is valid for all degrees of inversion and any back-gate bias conditions. In contrast, each drain

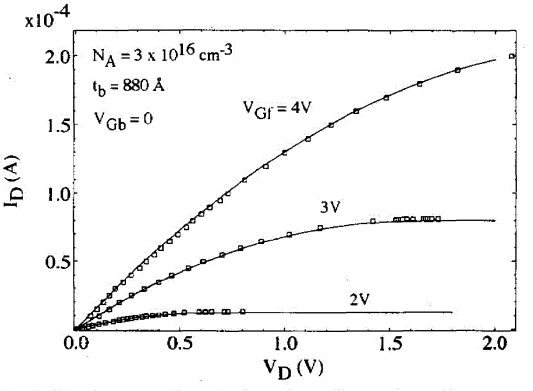

Fig. 3. Drain current vs drain voltage for various front-gate voltages, $V_{Gb}=0$, $Z=11.3\,\mu$m, $L=9.5\,\mu$m, $\mu_n=700\,\text{cm}^2\,\text{V}^{-1}.\text{s}^{-1}$, and the same remaining parameters used in Fig. 2. The squares are the rigorous results from the double integral relationship in eqn (11), and the solid lines are the results obtained from the single integral relationship in eqn (27).

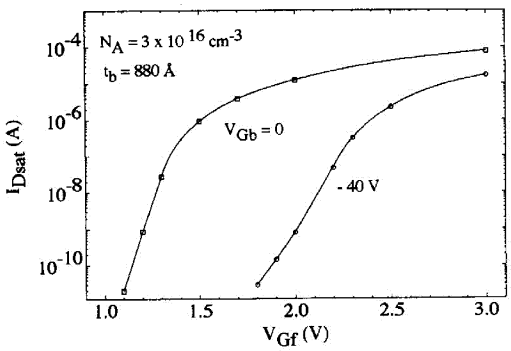

Fig. 4. The drain saturation current vs front-gate bias for two back-gate biases, and the same remaining parameters used in Fig. 3.

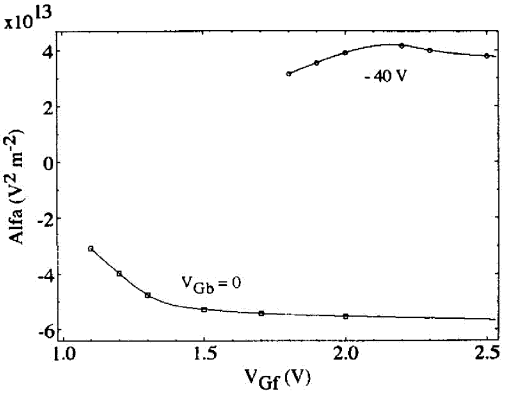

Fig. 6. Parameter α vs front-gate voltage for two back-gate biases, and the same parameters used to obtain the plots shown in Fig. 4. Parameter α relates the charge coupling effects between front- and back-gates.

current equation of the previously published models[2,3] is only valid for a given back-gate bias condition.

To confirm the equivalence of the double- and single-integral relationships, we compare the predicted current–voltage characteristics from eqn (27) with the rigorous result from eqn (11). Figure 3 shows I_D vs V_D for various V_{Gf}, $V_{Gb} = 0$, $Z = 11.3\,\mu$m, $L = 9.5\,\mu$m, $\mu_n = 700$ cm^2 V^{-1}s^{-1} (assuming, for this example, a constant effective mobility), and the same remaining parameters used in Fig. 2. We find in this figure a very good agreement between the results obtained from the double- and single-integral relationships.

Using a 386-based PC with a math coprocessor at 16 MHz and the two-dimensional bisection method[8–12], a typical calculation of the surface potentials (U_{sfL}, U_{sf0}, U_{sbL}, U_{sb0}, α_L and α_0) takes about 10 s; and from there the calculation of the drain current consumes less than 2 s.

To illustrate the charge coupling effects between front- and back-gates in thin-film SOI MOSFETs, Fig. 4 presents the drain saturation current I_{Dsat} vs V_{Gf} for two V_{Gb} and the same remaining parameters used in the previous figure. The behavior of $I_{Dsat}(V_{GF})$ presents two distinct dependencies: exponential for low values of V_{Gf} (weak inversion) and parabolic for high V_{Gf} (strong inversion). The parabolic dependence of $I_{Dsat}(V_{Gf})$, which is well explained by Lim and Fossum's analyses[2,7] for strong inversion, is used to estimate the front-gate threshold voltage V_{Tf}. We find that V_{Tf} changes from 1.35 to 2.21 V for a variation of V_{Gb} from 0 to -40 V.

The procedure for understanding the exponential dependence of $I_{Dsat}(V_{Gf})$, for weak inversion, is described as follows. First, since I_{Dsat} is basically only a diffusion current[4,21], I_{Dsat} is proportional to the inversion charge at source, $Q_n(y = 0)$. Second, $Q_n(y = 0)$ presents an exponential dependence[9] with respect to U_{sf}. Third, the linear dependence of U_{sf} on V_{Gf}, for weak inversion, is illustrated in Fig. 5, for the same parameters of the previous figure. Therefore, I_{Dsat} must be exponentially dependent on V_{Gf}.

We observe in Fig. 4 that the subthreshold slope of I_{Dsat} (V_{Gf}) changes from 63 to 140 mV decade^{-1}. This is due to the variation in the slope of $U_{sf}(V_{Gf})$, shown in Fig. 5. These two variations are highly related to the behavior of the variable α, which is presented in Fig. 6. We see, for $V_{Gb} = 0$, that α is negative, and the slope of $U_{sf}(V_{Gf})$ is 0.97. In contrast, for $V_{Gb} = -40$ V, α is positive, and the slope of $U_{sf}(V_{Gf})$

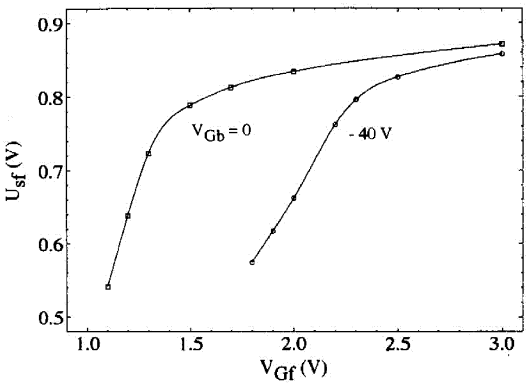

Fig. 5. The front-surface potential vs front-gate voltage for two back-gate biases, and the same parameters used to calculate the results of Fig. 4.

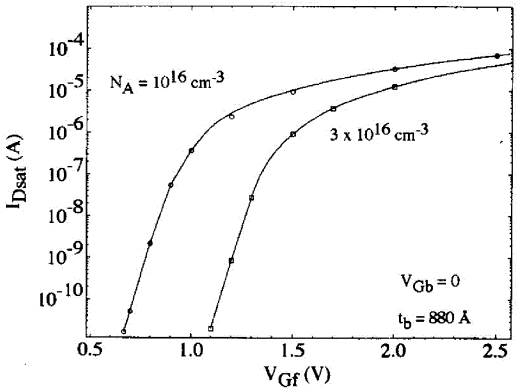

Fig. 7. The drain saturation current vs front-gate bias for two doping levels, $V_{Gb} = 0$, and the same remaining parameters used in the previous figures.

is 0.43. This tendency, in which the subthreshold slope of $I_{Dsat}(V_{Gf})$ increases as V_{Gb} decreases, has been observed experimentally by Ioannou[22] for fully-depleted n-channel SOI MOSFETs.

Figure 7 presents I_{Dsat} vs V_{Gf} for two doping levels, $V_{Gb} = 0$, and the same remaining parameters used to derive the plots in Fig. 3. We observe in this figure that the subthreshold slope of $I_{Dsat}(V_{Gf})$ presents a very weak dependence on N_A, and that V_{Tf} changes from 1.35 to 0.95 V for a variation of N_A from 3×10^{16} to 1×10^{16} cm^{-3}.

We present in Fig. 8 I_{Dsat} vs V_{Gf} for two film thickness, $V_{Gb} = 0$, and the same remaining parameters used in Fig. 3. For this variation of film thickness we find that the subthreshold slope of I_{Dsat} (V_{Gf}) is nearly constant, and that V_{Tf} changes from 1.35 to 1.74 V as t_b varies from 880 to 1500 Å. This is because the charge coupling effects decrease as t_b increases; therefore, V_{Tf} will approach the threshold voltage of the bulk device[21], which is 1.86 V for this particular case.

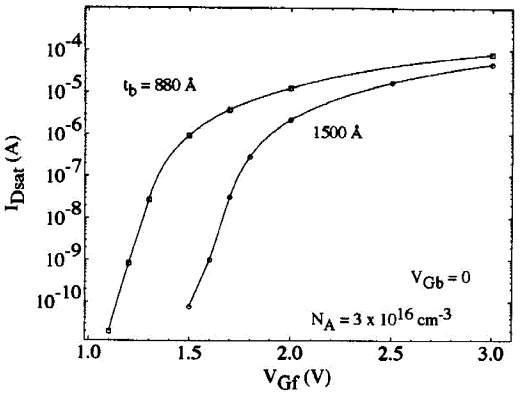

Fig. 8. The drain saturation current vs front-gate bias for two film thickness, $V_{Gb} = 0$, and the same remaining parameters used in Fig. 3.

3. CLOSED-FORM APPROXIMATIONS

We will analyze some particular cases of bias conditions to illustrate how our general result, described in eqn (27) by a single expression, contains the previous models of Pierret and Shields[1], Mallikarjun and Bhat[3] and Lim and Fossum[2,7]. These three models correspond to the following cases: (i) thick-film; (ii) thin-film with depletion approximation; and (iii) thin-film with depletion approximation and strong inversion condition.

3.1. The thick-film case

For very large values of t_b, the charge coupling between the front- and back-gate diminishes. Therefore, U_{sbL}, U_{sb0}, α_L and α_0 tend to zero, and eqn (27) simplifies to:

$$I_D = +\mu_n \frac{Z}{L}\left[C_{of}[V_{Gf}(U_{sfL} - U_{sf0}) - \tfrac{1}{2}(U_{sfL}^2 - U_{sf0}^2)] + \epsilon_s \int_0^{U_{sf0}} F(U, V = 0)\, dU - \epsilon_s \int_0^{U_{sfL}} F(U, V = V_D)\, dU \right], \quad (28)$$

which is exactly the Pierret and Shields equation[1] for long-channel bulk devices.

3.2. The thin-film case with depletion approximation

The solution of Poisson's equation with the boundary conditions $U(x = 0) = U_{sf}$ and $U(x = t_b) = U_{sb}$, assuming that the Si film is completely depleted[2,3,7], yields:

$$U(x) = \frac{qN_A}{2\epsilon_s} x^2 - F_{sfda} x + U_{sf} \quad (29)$$

and

$$F(x) = -\frac{qN_A}{\epsilon_s} x + F_{sfda} \quad (30)$$

where

$$F_{sfda} = +\left[\frac{U_{sf} - U_{sb}}{t_b} - \frac{Q_b}{2\epsilon_s}\right]. \quad (31)$$

The terms with the integrations in eqn (27) can be calculated by changing the variable:

$$\int_{U_{sb}}^{U_{sf}} F(U)\, dU = \int_{t_b}^{0} -F(x)^2\, dx, \quad (32)$$

in combination with eqns (30) and (31):

$$\epsilon_s \int_{U_{sb0}}^{U_{sf0}} F(U, V = 0)\, dU - \epsilon_s \int_{U_{sbL}}^{U_{sfL}} F(U, V = V_D)\, dU = C_b[(U_{sf0} - U_{sb0})^2 - (U_{sfL} - U_{sbL})^2], \quad (33)$$

where $C_b = \epsilon_s / t_b$ is the depletion capacitance.

The procedure to calculate the term with $(\alpha_L - \alpha_0)$ in eqn (27) is described as follows. First, the depletion approximation is used to estimate $G^2(U_{sf}, V)$, described in eqn (6):

$$G^2(U_{sf}, V) \approx \frac{2}{\beta L_D^2} U_{sf} \quad (34)$$

Second, the combination of the definition of the variable $\alpha = F_{sf}^2 - G^2(U_{sf}, V)$ in eqn (3) with eqns (31) and (34) gives the value of α. Third, the evaluation of α at drain and source yields:

$$\tfrac{1}{2}\epsilon_s t_b[\alpha_L - \alpha_0] = -\frac{C_b}{2}[(U_{sf0} - U_{sb0})^2 - (U_{sfL} - U_{sbL})^2] + \frac{Q_b}{2}[U_{sfL} + U_{sbL} - U_{sf0} - U_{sb0}]. \quad (35)$$

Finally, the substitution of eqns (33) and (35) into (27) gives:

$$I_D = +\mu_n \frac{Z}{L} C_{of}\left\{\left[V_{Gf} + \frac{Q_b}{2C_{of}}\right](U_{sfL} - U_{sf0}) - \tfrac{1}{2}(U_{sfL}^2 - U_{sf0}^2) + \frac{C_{ob}}{C_{of}}\left[\left[V_{Gb} + \frac{Q_b}{2C_{of}}\right] \times (U_{sbL} - U_{sb0}) - \tfrac{1}{2}(U_{sbL}^2 - U_{sb0}^2)\right] + \frac{C_b}{2C_{of}}[(U_{sf0} - U_{sb0})^2 - (U_{sfL} - U_{sbL})^2]\right]\right\}. \quad (36)$$

The above equation is valid if the film is completely depleted regardless of the back-gate bias conditions. Now we will compare our eqn (36), for some particular back-gate bias conditions, with the model of Mallikarjun and Bhat[3].

3.2.1. Back-surface accumulated from source to drain. If the back-surface is accumulated, then $U_{sb0} = U_{sbL} = 0$ and eqn (36) is simplified to:

$$I_D = +\mu_n \frac{Z}{L} C_{of}\left\{\left[V_{Gf} + \frac{Q_b}{2}\right] \times (U_{sfL} - U_{sf0}) - \tfrac{1}{2}\left[1 + \frac{C_b}{C_{of}}\right](U_{sfL}^2 - U_{sf0}^2)\right\}, \quad (37)$$

Which is equivalent to eqn (63) of Mallikarjun and Bhat[3], provided the condition $\beta V_{Gf} \gg (1 + C_b/C_{of})$ is satisfied.

3.2.2. *Back-surface depleted from source to drain.* There is a simple relationship[2,3,7] between U_{sf} and U_{sb} when the back-surface is depleted. This is obtained by equating $F(x = t_b)$ from eqn (30) and F_{sb} from eqn (2):

$$U_{sb}(y) = \frac{C_{ob}}{C_{ob} + C_b}\left[V_{Gb} + \frac{C_b}{C_{ob}} U_{sf}(y) + \frac{Q_b}{2C_{ob}}\right]. \quad (38)$$

The evaluation of eqn (38) at $y = 0$ ($U_{sb} = U_{sb0}$ and $U_{sf} = U_{sf0}$) and $y = L$ ($U_{sb} = U_{sbL}$ and $U_{sf} = U_{sfL}$), in combination with eqn (36) gives:

$$I_D = +\mu_n \frac{Z}{L} C_{of}\left\{\left[V_{Gf} + \frac{Q_b}{2C_{of}} + \frac{C_{bb}}{C_{of}}\left[V_{Gb} + \frac{Q_b}{2C_{ob}}\right]\right] \times (U_{sfL} - U_{sf0}) - \tfrac{1}{2}\left[1 + \frac{C_{bb}}{C_{of}}\right](U_{sfL}^2 - U_{sf0}^2)\right\}, \quad (39)$$

where C_{bb} is the series combination of C_{ob} and C_b [$C_{bb} = C_{ob}C_b/(C_{ob} + C_b)$]. The result presented in eqn (39) is equal to eqn (64) of Mallikarjun and Bhat's model[3] as long as the condition $\beta V_{Gf} \gg (1 + C_{bb}/C_{of})$ is fulfilled.

3.2.3. Back surface accumulated near source and depleted near drain. In contrast to the previous models[2,3], which need to evaluate the transition point between accumulation and depletion regions in the back surface, we analyze this case as a combination of the previous two cases. The back surface accumulation condition near the source implies that U_{sb0} is pinned at zero; and the depletion condition near the drain allows us to use eqn (38) to calculate U_{sbL} in terms of U_{sfL}. Finally, combining these two conditions with eqn (36) yields:

$$I_D = +\mu_n \frac{Z}{L} C_{of}\left\{\left[V_{Gf} + \frac{Q_b}{2C_{of}}\right](U_{sfa} - U_{sf0}) - \tfrac{1}{2}\left[1 + \frac{C_b}{C_{of}}\right](U_{sfa}^2 - U_{sf0}^2) + \left[V_{Gf} + \frac{Q_b}{2C_{of}} + \frac{C_{bb}}{C_{of}} \times \left[V_{Gb} + \frac{Q_b}{2C_{ob}}\right]\right](U_{sfL} - U_{sfa}) - \tfrac{1}{2}\left[1 + \frac{C_{bb}}{C_{of}}\right](U_{sfL}^2 - U_{sfa}^2)\right\} \quad (40)$$

where

$$U_{sfa} = -\frac{C_{ob}}{C_b}\left[V_{Gb} + \frac{Q_b}{2C_{ob}}\right]. \quad (41)$$

The result shown in eqn (40) is identical to eqn (61) of Mallikarjun and Bhat's model[3] provided the condition $\beta V_{Gf} \gg (1 + C_b/C_{of})$ is satisfied.

3.3. The thin-film case with depletion approximation and strong inversion condition

For this case we use the strong inversion approximation, which establishes $U_{sf0} = 2\phi_B$ and $U_{sfL} = 2\phi_B + V_D$, in combination with: (i) eqn (37), if the back surface is accumulated from source to drain; (ii) eqn (39), if the back surface is depleted from source to drain; or (iii) eqn (40), if the back surface is accumulated near the source and depleted near the drain. The results of this analysis yield Lim and Fossum's three current equations published in 1984[2].

4. CONCLUSIONS

A single-integral expression, valid for any front- and back-gate bias condition, has been obtained to describe the current–voltage characteristics for the long-channel SOI MOSFET. This relationship includes the diffusion component of the drain current and is valid from weak to strong inversion. It was obtained from the transformation of a double-integral expression by a procedure analogous to that of Pierret and Shields[1] for the long-channel bulk MOSFET. The evaluation of this single-integral expression is an attractive way to calculate the drain current, at any level of inversion, because of the significant simplification involved in the computation.

This single-integral relationship yields: (i) Lim and Fossum's model[2], if the strong inversion condition and the depletion approximation are used; (ii) Mallikarjun and Bhat's model[3], if only the depletion approximation is incorporated; and (iii) Pierret and Shields' equation[1] for a bulk device, if the Si film is very thick.

Finally, we would like to stress that our theory, which is valid for a long-channel device at any bias condition, is the first step towards the development of a general model for short-channel devices.

Acknowledgements—The authors would like to express their gratitude to one of the reviewers for useful comments. Financial support for this work was provided by the U.S. National Science Foundation through Grant INT 9002077, the Venezuelan "Consejo Nacional de Investigaciones Científicas y Tecnológicas", and by "Universidad Simón Bolívar" through "Decanato de Investigaciones".

REFERENCES

1. R. F. Pierret and J. A. Shields, *Solid-St. Electron.* **26,** 143 (1983).
2. H.-K. Lim and J. G. Fossum, *IEEE Trans. Electron Devices* **ED-31,** 401 (1984).
3. C. Mallikarjun and K. N. Bhat, *IEEE Trans. Electron Devices* **ED-37,** 2039 (1990).
4. J. P. Colinge, *Silicon-on-Insulator Technology: Materials to VLSI.* Kluwer, (1991).
5. M. Yoshimi, H. Hazama, M. Takahashi, S. Kambayashi, T. Wada, K. Kato and H. Tango, *IEEE Trans. Electron Devices* **ED-36,** 493 (1989).
6. M. Yoshimi, M. Takahashi, T. Wada, K. Kato, S. Kambayashi, M. Kemmochi and K. Natori, *IEEE Trans. Electron Devices* **ED-37,** 2015 (1990).
7. H.-K. Lim and J. G. Fossum, *IEEE Trans. Electron Devices* **ED-30,** 1244 (1983).
8. A. Ortiz-Conde, F. J. García Sánchez, P. E. Schmidt and A. Sa-Neto, *Solid-St. Electron.* **31,** 1497 (1988).
9. A. Ortiz-Conde, F. J. García Sánchez, P. E. Schmidt and A. Sa-Neto, *IEEE Trans. Electron Devices* **ED-36,** 1651 (1989).
10. A. Ortiz-Conde, F. J. García Sánchez, P. E. Schmidt and A. Sa-Neto, *Proc. Twentieth Modeling and Simulation Conf.*, Vol. 20, p. 1341 (1989).
11. A. Ortiz-Conde, F. J. García Sánchez, P. E. Schmidt, A. Sa-Neto, J. Andrian and J. Muci, *Proc. Twenty-first Modeling and Simulation Conf.*, Vol. 21, p. 1689 (1990).
12. A. Ortiz-Conde, P. E. Schmidt, F. J. García Sánchez, R. Herrera and J. Andrian, *Proc. Int. Semiconductor Device Research Symp.*, Vol. 1, p. 613 (1991).
13. J. B. McKitterick and A. L. Caviglia, *IEEE Trans. Electron Devices* **ED-36,** 1133 (1989).
14. M. Schubert, B. Hofflinger and R. P. Zing, *Solid-St. Electron.* **33,** 1553 (1990).
15. J. R. Brews, *Solid-St. Electron.* **21,** 345 (1978).
16. G. Baccarani, M. Rudan and G. Spadini, *IEEE J. Solid-St. Electron Devices* **2,** 62 (1978).
17. J. R. Brews, *Applied Solid State Science, Supplement* 2*A*. Academic Press, New York (1981).
18. Y. Tsividis, *Solid-St. Electron.* **25,** 1099 (1982).
19. H. C. Pao and C. T. Sah, *Solid-St. Electron.* **9,** 927 (1966).
20. D. Flandre and F. Van de Wiele, *IEEE Electron Device Lett.* **EDL-9,** 296 (1988).
21. R. M. Warner and B. L. Grung, *Transistors Fundamentals for the Integrated-circuit Engineer.* Wiley-Interscience, New York (1983).
22. D. E. Ioannou, *Proc. Int Semiconductor Device Research Symp.*, Vol. 1, p. 151 (1991).